Society of Medical Education & Research

2021, Volume 1, Page No: 193-118
ISSN: 3108-4834

Archive of International Journal of Cancer and Allied Science

Influence of OASL on Oxaliplatin-Triggered Immunogenic Cell Death in Gastric Cancer Through the cGAS-STING Signaling Pathway

Laura Katherine Mitchell[1], Hannah Olivia Brooks[1]*, David Andrew Collins[2], Peter Jonathan Moore[2], Samuel Edward Wright[3], Oliver Thomas Green[3]

[1]Department of Oncology, University of Oxford, Oxford, United Kingdom.
[2]Cancer Research UK Cambridge Institute, University of Cambridge, Cambridge, United Kingdom.
[3]Institute of Cancer Research, London, United Kingdom.

***E-mail** ✉ h.brooks.oncology@gmail.com

Abstract

This study explores the regulatory role of 2'-5' oligoadenylate synthetase-like (OASL) in modulating oxaliplatin (OXA)-induced immunogenic cell death (ICD) in gastric cancer (GC) via the cGAS-STING signaling pathway. Silencing OASL resulted in increased ICD expression, whereas its overexpression suppressed these effects. Transcriptomic profiling of OASL-knockdown and control GC cells treated with OXA demonstrated marked enrichment in the cGAMP-mediated second messenger pathway. As a key upstream enzyme, cGAS generates the second messenger cGAMP, which directly activates STING. Mechanistic investigations confirmed that OASL regulates OXA-induced ICD in GC cells through the cGAS-STING pathway. Co-immunoprecipitation and immunofluorescence assays revealed a direct interaction between OASL and cGAS proteins. These findings were further corroborated in an in vivo mouse model. Collectively, the data indicate that OASL modulates OXA-induced ICD via cGAS-STING, influencing chemosensitivity, and highlight OASL as a potential target for enhancing OXA efficacy in GC treatment.

Keywords: Gastric cancer, Oxaliplatin, Immunogenic cell death, cGAS-STING signaling pathway, 2'-5' oligoadenylate synthetase-like

Introduction

Gastric cancer (GC) ranks as the fifth most prevalent malignancy globally and is the fourth leading cause of cancer-related mortality, with high incidence in China [1, 2]. Despite advances in both basic and clinical research, including novel chemotherapeutic regimens, targeted therapies, and immunotherapies, prognosis for GC patients remains unsatisfactory [3-6]. Chemotherapy continues to be a cornerstone in the management of advanced GC [7]. Although OXA-based regimens improve survival outcomes, clinical response rates remain limited to approximately 40–67% [8, 9], and the development of drug resistance is a major challenge. Evidence suggests that modulating specific molecular pathways can restore OXA sensitivity in GC cells. For instance, JUNB enhances resistance via MAPK pathway activation, reversible with ERK/MEK inhibitors [10]; EphA2 mediates resistance through EMT induction, which can be reversed by gene silencing [11]; at the epigenetic level, METTL3 maintains CD133+ stem cell resistance by promoting DNA base excision repair and stabilizing PARP1 mRNA [12, 13]. Additionally, autophagy regulation via the LINC00641/miR-582-5p axis contributes to OXA resistance, and its inhibition increases OXA cytotoxicity [14]. However, these markers are not yet widely applied in clinical settings [15, 16], underscoring the need for in-depth molecular studies of GC.

Access this article online https://smerpub.com/

Received: 12 January 2021; **Accepted:** 11 March 2021

How to cite this article: Mitchell LK, Brooks HO, Collins DA, Moore PJ, Wright SE, Green OT. Influence of OASL on Oxaliplatin-Triggered Immunogenic Cell Death in Gastric Cancer Through the cGAS-STING Signaling Pathway. Arch Int J Cancer Allied Sci. 2021;1:103-18. https://doi.org/10.51847/nr4Epz4CW0

The 2′-5′ oligoadenylate synthetase (OAS) family, an interferon-stimulated gene group, comprises OAS1, OAS2, OAS3, and ubiquitin-like OASL. Unlike other family members, OASL lacks enzymatic synthetase activity but possesses an N-terminal oligoadenylate-like domain and two C-terminal ubiquitin-like domains essential for its antiviral function [17-20]. Emerging evidence indicates that OASL is critical for immune regulation and drug metabolism [21-23]. Recent studies have linked OASL to cancer progression and prognosis, including in breast [24], pancreatic [25], and cervical cancers [26]. Previous work from our group demonstrated that OASL promotes proliferation, invasion, and migration while inhibiting apoptosis in GC cells, functioning as an oncogene in GC development [27]. OASL also appears to influence chemotherapeutic sensitivity, as observed in lung cancer, suggesting that its modulation could enhance drug efficacy [28]. Moreover, OAS family members have been identified as key genes in trastuzumab-resistant GC [29], highlighting OASL's potential role in maintaining treatment responsiveness.

Beyond direct cytotoxicity, OXA exerts anti-tumor effects by modulating immune responses, including ICD induction, STAT pathway modulation, and tumor microenvironment regulation [30-35]. Based on these insights, we hypothesized that OASL could play a pivotal role in governing OXA sensitivity in GC through immunogenic mechanisms. In this study, GC cells subjected to OASL knockdown or overexpression were treated with OXA, revealing that OASL suppression enhanced ICD, whereas overexpression inhibited it. Subsequent mRNA sequencing of OASL-knockdown and control GC cells treated with OXA for 24 hours demonstrated significant enrichment in cGAMP-mediated signaling, suggesting that OASL influences OXA-induced ICD via the cGAS-STING pathway. These findings provide a rationale for targeting OASL to improve chemotherapeutic responses in GC.

Materials and Methods

Cell culture

Gastric cancer (GC) cell lines AGS, MKN45, and HGC27 were obtained from Cobioer (Nanjing, China) and maintained in RPMI 1640 medium (BasalMedia, Shanghai, China) supplemented with 10 percent fetal bovine serum (FBS) in a humidified incubator at 37°C with 5% CO_2. Cells were treated with oxaliplatin (OXA, S1224, Selleck, China), the STING inhibitor H151 (S6652, Selleck, China), or the STING agonist diABZI (Compound 3, S8796, Selleck, China) as indicated.

Cell transfection

siRNAs targeting OASL (si-OASL: CCATCACGGTCACCATTGT) and STING (si-STING: GGUCAUAUUACAUCGGAUA), along with a negative control siRNA (si-NC), were purchased from RiboBio (Guangzhou, China). OASL cDNA was cloned into the pcDNA3.1 vector (Tsingke Biotechnology, Beijing, China). AGS and MKN45 cells were transfected with si-OASL or si-NC, while HGC27 cells were transfected with empty vector or pcDNA3.1-OASL using Lipofectamine 2000 (Invitrogen, USA). Transfection efficiency was evaluated 48 hours later using RT-qPCR and western blotting.

Cell viability assay (CCK-8)

AGS, MKN45, and HGC27 cells were seeded in 96-well plates at a density of 5×10^3 cells per well. Following treatment, CCK-8 reagent (Beyotime, Shanghai, China) was added and incubated for 2 hours, after which absorbance at 450 nm was measured using a Bio-Rad microplate reader (USA).

Apoptosis analysis by flow cytometry

Cells were washed with PBS and digested with 0.25% trypsin. After centrifugation at 1000 g for 5 minutes, cells were resuspended in PBS and counted. A total of 2×10^5 cells per well were incubated with 195 µL Annexin V-FITC binding solution, followed by 5 µL Annexin V-FITC and 10 µL propidium iodide (PI). After 20 minutes incubation in the dark at 37°C, apoptosis was quantified by flow cytometry.

Flow cytometric analysis of surface calreticulin (CRT)

AGS, MKN45, and HGC27 cells were seeded in 6-well plates and harvested post-treatment. Cells were washed twice with cold PBS and incubated with primary anti-CRT antibody at 4°C for 60 minutes in the dark. After washing, fluorophore-conjugated secondary antibody was added for 30 minutes at room temperature, followed by two additional PBS washes. Cells were resuspended in 300–500 µL PBS and analyzed by flow cytometry.

Dendritic cell (DC) co-culture and maturation assay

Human DCs were differentiated from peripheral blood mononuclear cells (PBMCs) via density gradient centrifugation and cultured in RPMI-1640/10% FBS

with GM-CSF (50 ng/mL) and IL-4 (20 ng/mL) for 5 days. Conditioned media were collected from AGS, MKN45, and HGC27 cells transfected with si-OASL or OASL and treated with 40 μM OXA for twenty four hours. DCs were exposed to 50% conditioned media for 24 hours at 37°C with 5% CO_2, and maturation was assessed by flow cytometric detection of CD80 and CD86 surface expression.

Western blotting

Proteins were extracted using RIPA lysis buffer (Beyotime, Shanghai, China), quantified with a BCA assay kit (Beyotime, Shanghai, China), separated by 10 percent SDS-PAGE, and transferred to PVDF membranes. Membranes were incubated overnight at 4°C with primary antibodies and then with HRP-conjugated secondary antibodies (ab205718, Abcam, USA) for 2 hours at room temperature. Protein bands were visualized using ECL (Beyotime, Shanghai, China) and quantified with ImageJ. Primary antibodies included: OASL (ab229136, Abcam, UK), cGAS (ab224144, Abcam, UK), STING (ab252560, Abcam, UK), IRF3 (ab245341, Abcam, UK), CRT (ab227444, Abcam, UK), HSP70 (ab194360, Abcam, UK), HSP90 (ab203126, Abcam, UK), CD8 (ab316778, Abcam, UK), GAPDH (10494-1-AP, Proteintech, USA), p-STING (AP1369, ABclonal, CN), p-TBK1 (AP1026, ABclonal, CN), and p-IRF3 (AP0995, ABclonal, CN).

Co-immunoprecipitation (Co-IP)

Cells were collected 48 hours post-transfection, washed with cold PBS, lysed on ice for 30 minutes, and sonicated for 3 minutes. After centrifugation, the supernatant was incubated with Protein A/G PLUS Agarose (15 μL, Beyotime, Shanghai, China) for 1 hour at 4°C. Antibodies (1.5 μg) were added to lysates and incubated for 1 hour at 4°C, followed by overnight incubation with Protein A/G agarose beads (40 μL) at 4°C. Beads were washed four times, boiled with loading buffer, and analyzed by western blot.

ELISA

Cell supernatants were collected and analyzed for HMGB1 levels using the corresponding ELISA kit (Beyotime, Shanghai, China) according to the manufacturer's instructions.

Extracellular ATP measurement

ATP released into the culture medium was quantified using a colorimetric ATP detection kit (Beyotime, Shanghai, China) following treatment.

Lactate dehydrogenase (LDH) assay

Cell culture supernatants were collected, and LDH levels were measured using an LDH detection kit (Beyotime, Shanghai, China) as per the kit protocol.

Immunofluorescence

Cells were fixed with 4 percent paraformaldehyde for ten minutes, permeabilized with 0.5% Triton X-100 for twenty minutes at room temperature, blocked, and incubated with primary antibodies for 1 hour. After labeling with fluorescent secondary antibodies, nuclei were counterstained with DAPI, and cells were visualized and imaged under a fluorescence microscope.

Mouse tumor model

Twenty male C57/BL6 mice (6–8 weeks old) were obtained from Jinan Pengyue Experimental Animal Breeding Co. Ltd. and maintained under SPF conditions with sterilized feed and autoclaved water. After one week of acclimatization in a controlled environment, mice were randomly divided into four experimental groups (n = 5 per group): sh-NC, sh-OASL, OXA + sh-NC, and OXA + sh-OASL. The sh-OASL construct (GAGTGTGACTAACAGAGTACC) was sourced from RiboBio (Guangzhou, China).

MFC cells transfected with the appropriate constructs were adjusted to 1.5×10^6 cells/mL, and 0.2 mL of the cell suspension was injected subcutaneously into the right axilla of each mouse. Tumor formation was confirmed when the diameter reached approximately 0.5 cm. OXA treatment was administered intraperitoneally at 10 mg/kg every 2 days (0.2 mL per dose), calculated based on the human-to-mouse surface area conversion factor (0.002:6). Tumor dimensions were recorded every three days using the formula: volume = (length × width^2)/2. Mice were euthanized on day 15, and tumors were excised, weighed, photographed, and sectioned: one portion for protein extraction and western blot, one for TUNEL staining, and the remaining tissue for CD8 immunohistochemistry.

Statistical analysis

All data analyses were performed with GraphPad Prism 17. Results are presented as mean ± standard deviation (SD). Student's t-test was applied to compare differences

between two groups, and statistical significance was defined as $P < 0.05$. Experiments were conducted in triplicate.

Results and Discussion

Oxaliplatin triggers immunogenic cell death in gastric cancer

Impact of oxaliplatin on GC cell growth and apoptosis

AGS, MKN45, and HGC27 cells were treated with a range of OXA concentrations (0, 5, 10, 20, 40, 80, 160 μM) for 24, 48, and 72 hours. CCK-8 assays revealed a clear time- and dose-dependent suppression of cell proliferation **(Figure 1a)**. Flow cytometry using Annexin V-FITC/PI staining showed a significant increase in apoptotic cell populations after 48 hours of treatment with 0–40 μM OXA ($P < 0.001$; **(Figure 1b)**), confirming OXA's pro-apoptotic effect.

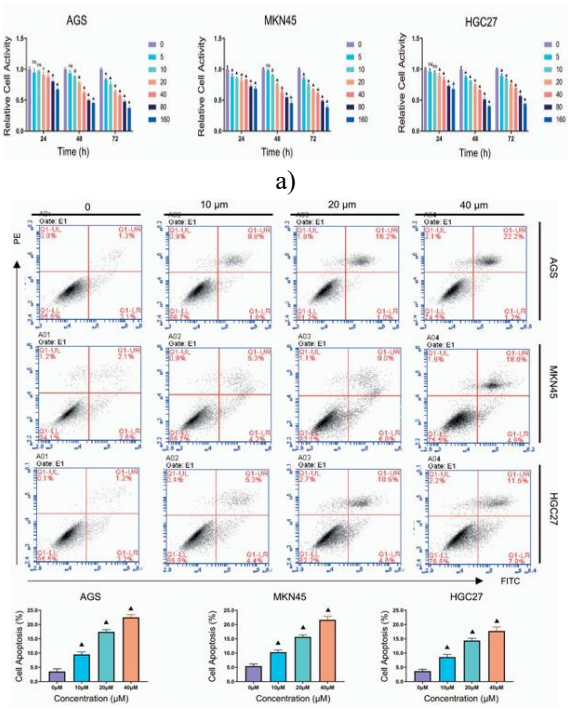

Figure 1. Effect of OXA on the proliferation and apoptosis of GC cells

(a) AGS,MKN45, and HGC27 cells were treated with OXA at various concentrations (0, 5, 10, 20, 40, 80, and 160 μM) for 24, 48, and 72 hours. The proliferation of GC cells was assessed using the CCK-8 assay. (b) AGS,MKN45,and HGC27 cells were treated with OXA at various concentrations (0, 10, 20, and 40 μM) for 48 hours. The apoptosis rates of GC cells were measured using flow cytometry with the Annexin-FITC/PI double staining method. The values indicate the mean±standard deviation (SD) of three independent experiments.Statistical significance is indicated as follows: "ns" indicates no statistically significant difference, "*" indicates $P < 0.05$, "#" indicates $P < 0.01$, and "▲" indicates $P < 0.001$.

Oxaliplatin-induced ICD in GC cells

ICD is characterized by the extracellular release of DAMPs such as calreticulin (CRT), HMGB1, and ATP. GC cells exposed to OXA (0, 10, 20, 40 μM) for 48 hours demonstrated dose-dependent CRT translocation from the cytoplasm to the plasma membrane, observed via immunofluorescence **(Figures 2a and 2b)**. ELISA assays of cell culture supernatants showed elevated HMGB1 ($P < 0.01$) and ATP ($P < 0.001$) in treated groups compared to untreated controls **(Figures 2c and 2d)**. Western blotting further indicated dose-dependent upregulation of HSP70 and HSP90 proteins ($P < 0.001$; **(Figure 2e)**).

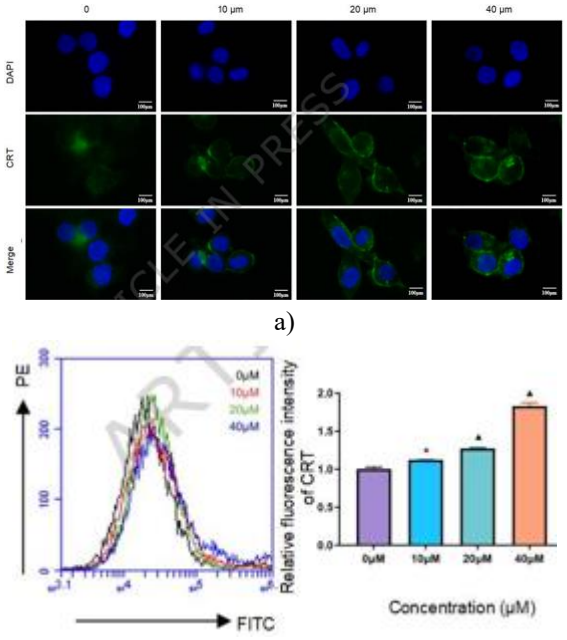

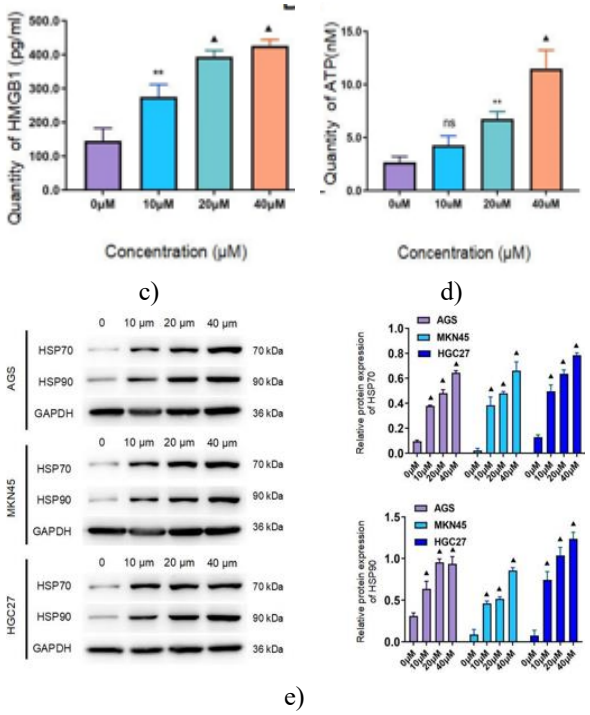

Figure 2. OXA induces immunogenic cell death in GC cells

(a) AGS cells were treated with OXA at various concentrations (0,10,20, and 40 μM) for 48 hours. The changes in CRT were observed via immunofluorescence. (b) AGS cells were treated with OXA at various concentrations (0,10,20,and 40 μM) for 48 hours.The expression level of CRT on cell membrane was measured using flow cytometry with dead cells,and a statistical chart was generated. (c) AGS cells were treated with OXA at various concentrations (0,10,20,and 40 μM) for 48 hours. The content of HMGB1 in the cell supernatant was measured using ELISA, and a statistical chart was generated.(d) AGS cells were treated with OXA at concentrations(0,10,20,and 40 μM) for 48 hours. The ATP content in the supernatant was quantified using ATP assay kit, and a statistical chart was generated. (e) AGS, MKN45, and HGC27 cells were treated with OXA at various concentrations (0,10,20,and 40 μM) for 48 hours. Western blot analysis was performed to assess the expression levels of HSP70 and HSP90 proteins, and a statistical chart was generated.The values indicate the mean±standard deviation (SD) of three independent experiments. Scale bar: 100 μm. Statistical significance is indicated as follows: "ns" indicates no statistically significant difference, "*" indicates $P < 0.05$,"**" indicates $P < 0.01$, and "▲" indicates $P < 0.001$.

OASL attenuates oxaliplatin-induced ICD

Modulation of apoptosis by OASL

To assess the relationship between OXA and OASL expression, AGS, MKN45, and HGC27 cells were treated with increasing OXA concentrations (0, 10, 20, 40 μM) for 48 hours. Western blot analysis revealed a dose-dependent increase in OASL protein levels ($P < 0.001$; **(Figure 3a)**), while RT-qPCR confirmed corresponding elevations in OASL mRNA ($P < 0.05$; **(Figure 3b)**).

The functional role of OASL in OXA-induced cytotoxicity was evaluated next. Knockdown of OASL in AGS and MKN45 cells followed by OXA treatment (0–40 μM) for 48 hours led to significantly higher apoptotic rates compared with control cells, as measured by Annexin V-FITC/PI flow cytometry ($P < 0.05$; **(Figure 3c)**). LDH release assays corroborated the enhanced cytotoxicity in OASL-deficient cells ($P < 0.05$; **(Figure 3e)**). Conversely, overexpression of OASL in HGC27 cells exposed to 40 μM OXA resulted in reduced apoptosis and LDH release ($P < 0.05$; **(Figures 3d and 3e)**). Collectively, these data indicate that OASL suppresses OXA-induced apoptosis and diminishes GC cell chemosensitivity.

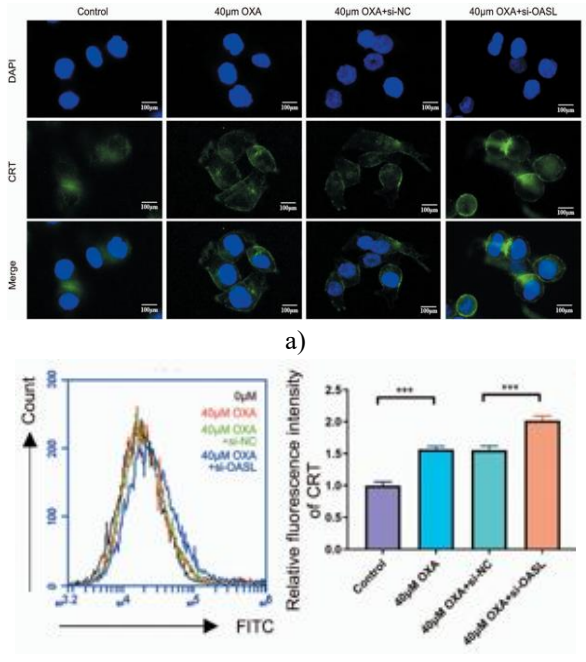

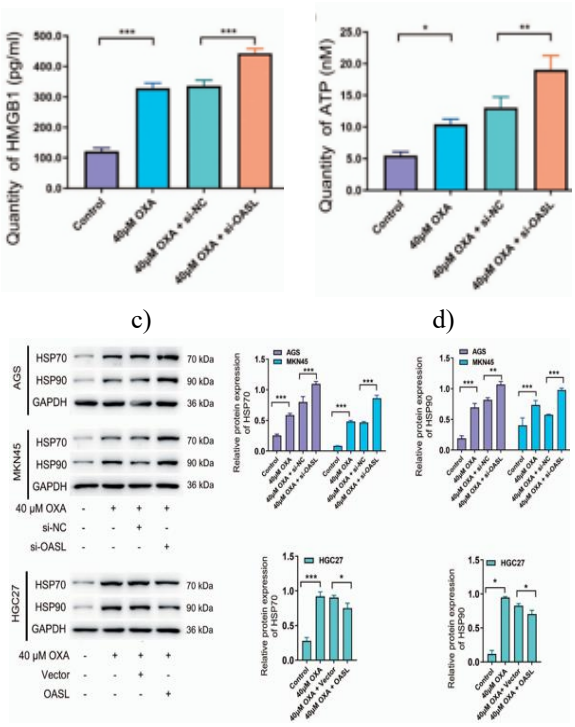

Figure 3. The Effect of OASL on OXA-induced apoptosis in GC cells

(a) AGS, MKN45, and HGC27 cells were treated with OXA at various concentrations (0,10,20, and 40 μM) for 48 hours. The **μWm** estern blot analys**10**i**0**s**μ** was performed to assess the protein expression levels of OASL in GC cells, followed by statistical analysis. (b) AGS, MKN45, and HGC27 cells were treated with OXA at various concentrations (0,10,20,and 40 μM) for 48 hours. RT-PCR was then utilized to measure OASL mRNA expression levels in the GC cells, followed by statistical analysis. (c) AGS cells underwent OASL knockdown and were subsequently treated with OXA at different concentrations (0,10,20,and 40 μM) for 48 hours. The apoptosis rate was measured by flow cytometry using the Annexin FITC/PI double staining method, and a statistical analysis of the apoptosis rate was conducted. (d) HGC27 cells were overexpressed with OASL and then treated with 40 μM OXA for 48 hours. Flow cytometry (using the Annexin FITC/PI double staining method) was employed to measure the apoptosis rate of AGS cells, along with the generation of a statistical chart reflecting the apoptosis rate. (e) Statistical graphs showed LDH content in AGS and MKN45 cells after OASL knockdown, followed by treatment with OXA at various concentrations (0,10,20,and 40 μM) for 48 hours, as well as in HGC27 cells after OASL overexpression followed by treatment with 40 μM OXA for 48 hours. The values indicate the mean±standard deviation (SD) of three independent experiments.Statistical significance is indicated as follows: "ns" indicates no statistically significant difference, "*" indicates $P < 0.05$, "**" indicates $P < 0.05$, and "▲" indicates $P < 0.001$.

Impact of OASL on oxaliplatin-induced immunogenic cell death in gastric cancer

To investigate the role of OASL in OXA-triggered ICD, AGS and MKN45 cells were treated with 40 μM OXA in combination with si-OASL for 48 hours, whereas HGC27 cells received 40 μM OXA along with OASL overexpression for the same duration. Western blot analysis confirmed that OXA treatment led to a marked upregulation of OASL in both experimental models ($P < 0.01$).

The influence of OASL on ICD-associated DAMPs was further examined in AGS and MKN45 cells. Cells were divided into four groups: control, OXA alone, OXA+si-NC, and OXA+si-OASL, with OXA applied at 40 μM for 48 hours. Analysis revealed that knockdown of OASL significantly enhanced ICD markers, including CRT accumulation on the cell membrane, elevated extracellular HMGB1 and ATP levels, and increased intracellular HSP70 and HSP90 expression compared with the OXA+si-NC group ($P < 0.05$; **(Figures 4a–4e)**). Similar trends were observed in MKN45 cells ($P < 0.05$). Conversely, overexpression of OASL in HGC27 cells treated with 40 μM OXA for 48 hours resulted in a substantial reduction of these ICD-associated DAMPs ($P < 0.05$). Collectively, these findings indicate that OASL acts as a negative regulator of OXA-induced ICD in gastric cancer cells.

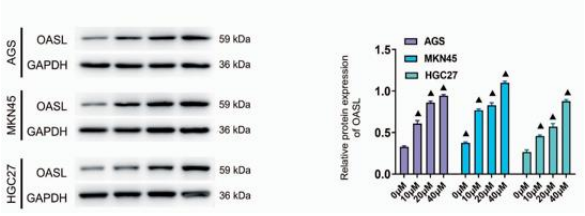

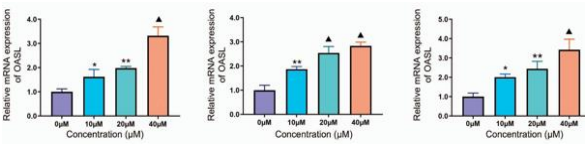

b)

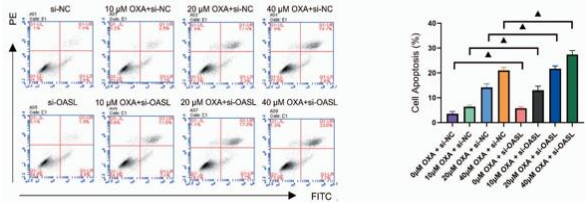

c)

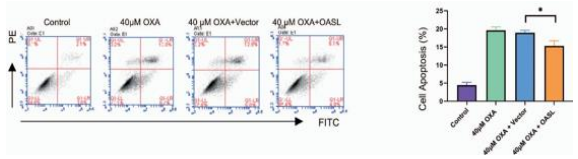

d)

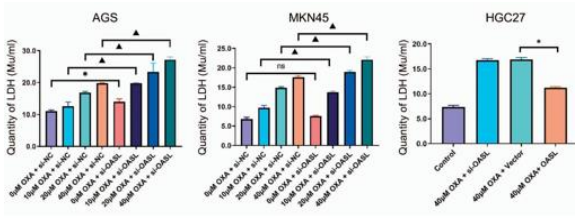

e)

Figure 4. OASL can reduce OXA-induced immunogenic cell death in GC cells

(a) AGS cells were treated with 40 μM OXA combined with si-OASL for 48 hours, and changes in CRT were observed using immunofluorescence. (b) AGS cells were treated with 40 μM OXA combined with si-OASL for 48 hours, the expression level of CRT on cell membrane was measured using flow cytometry with dead cells,and a statistical chart was generated. (c)AGS cells were treated with 40 μM OXA combined with si-OASL for 48 hours, and the statistical plot of HMGB1 content in cell supernatant of cell culture medium was detected using ELISA assay. (d) AGS cells were treated with 40 μM OXA combined with si-OASL for 48 hours, and statistical plot of ATP content in cell supernatant of cell culture medium was detected using ATP kit. (e) AGS and MKN45 cells were treated with 40 μM OXA in combination with si-OASL for 48 hours, and HGC27 cells were treated with 40 μM OXA in combination with overexpression of OASL for 48 hours. The expression levels of HSP70 and HSP90 protein in AGS,MKN45, and HGC27 cells were determined by Western blot, and statistical graphs were obtained. The values indicate the mean±standard deviation (SD) of three independent experiments.Scale bar: 100 μm. Statistical significance is indicated as follows: "*" indicates $P < 0.05$, "**" indicates $P < 0.01$, and "***" indicates $P < 0.001$.

OASL suppresses oxaliplatin-induced ICD via the cGAS-STING pathway

Previous data suggested that OASL promotes proliferation, migration, and invasion of GC cells while inhibiting ICD, thereby reducing sensitivity to OXA. To elucidate the underlying molecular mechanisms, we focused on the potential involvement of the cGAS-STING signaling pathway.

Identification of downstream pathways via mRNA sequencing

To explore the mechanisms by which OASL inhibits ICD, mRNA sequencing was performed on MKN45 cells comparing OXA+si-NC versus OXA+si-OASL treatment. Differential gene expression was visualized using a heatmap **(Figure 5a)** and a volcano plot revealed 1,243 significantly dysregulated genes **(Figure 5b)**. Reactome pathway enrichment indicated a strong association with the cGAMP second messenger pathway, highlighting the central role of cGAS-mediated cGAMP production and subsequent STING-dependent immune activation **(Figure 5c)**. These data suggest that OASL modulates ICD through the cGAS-STING pathway.

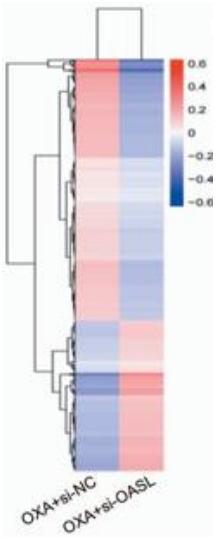

a)

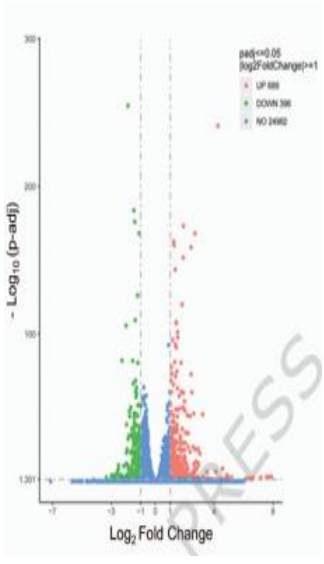

b)

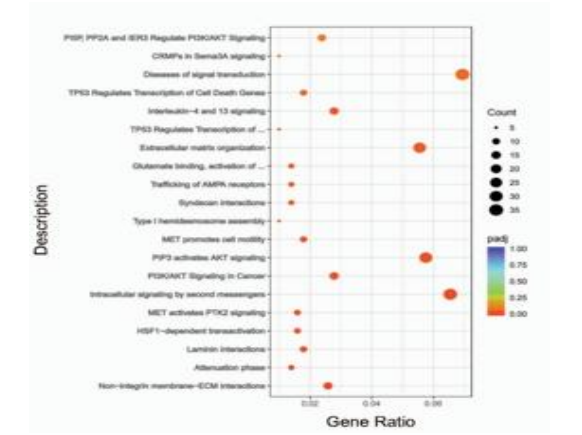

c)

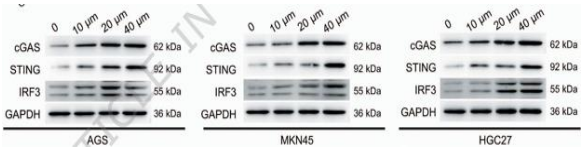

d)

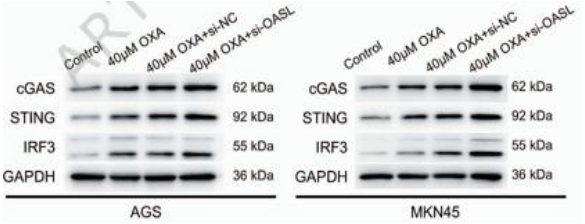

e)

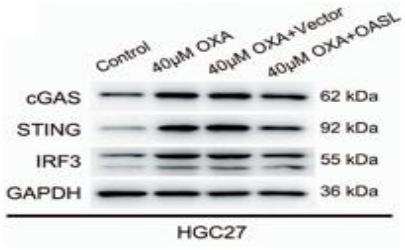

f)

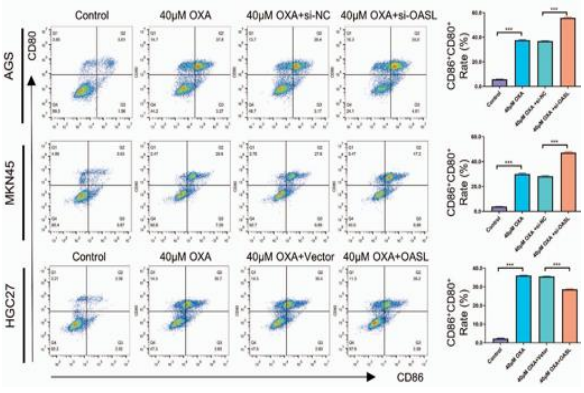

g)

Figure 5. OASL regulates the expression of key proteins in the cGAS-STING signaling pathway

(a) All the detected mRNA expression levels were visualized using the heatmap(n=3). (b) The Intervention up-regulated and down-regulated mRNA were displayed in groups using a volcano map. (c) Reactome enrichment analysis of the differential mRNA.Reactome enrichmentanalysis of the differentially expressed genes showed significant enrichment in intracellular signaling by second messenger,The cGAS recognizes and binds DNA in the cytoplasm, catalyzes the synthesis of ATP and GTP into cGAMP; cGAMP acts as a second messenger to bind and activate STING.

(d) AGS, MKN45, and HGC27 cells were treated with OXA at various concentrations (0,10,20, and 40 μM) for 48 hours, and the expression levels of key proteins of the cGAS-STING signaling pathway were determined by Western blot.(e) AGS and MKN45 cells were treated with 40 μM OXA combined with si-OASL for 48 hours, HGC27 cells were treated with 40 μM OXA in combination with overexpression of OASL for 48 hours, and the expression levels of key proteins of the cGAS-STING signaling pathway were determined by Western blot.(f)AGS and MKN45 cells were treated with 40 μM OXA combined with si-OASL for 48 hours, HGC27 cells were treated with 40 μM OXA in combination with overexpression of OASL for 48 hours, and then co-culture with immature DC cells, and the expression level of CD86/CD80 on the surface of DC cells were detected using by flow cytometry,and statistical graphs were obtained. The values indicate the mean±standard deviation (SD) of three independent experiments.Statistical significance is indicated as follows: "***" indicates $P < 0.001$.

Modulation of key cGAS-STING proteins by OASL

To examine the connection between OXA and the cGAS-STING pathway, AGS, MKN45, and HGC27 cells were treated with escalating doses of OXA (0, 10, 20, 40 μM) for 48 hours. Western blot analysis demonstrated dose-dependent increases in cGAS, STING, IRF3, P-STING, P-TBK1, and P-IRF3 protein levels relative to untreated controls ($P < 0.05$; **(Figure 5d)**), confirming that OXA activates the cGAS-STING signaling cascade.

Next, the impact of OASL on pathway activation was assessed. AGS and MKN45 cells transfected with si-OASL or controls were treated with 40 μM OXA for 48 hours. Knockdown of OASL led to enhanced expression

of cGAS, STING, IRF3, P-STING, P-TBK1, and P-IRF3 compared to OXA+si-NC cells ($P < 0.05$; **(Figure 5e)**). Conversely, HGC27 cells overexpressing OASL exhibited decreased levels of these proteins following OXA treatment ($P < 0.05$; **(Figure 5f)**).

To evaluate functional consequences on immune cells, immature dendritic cells (DCs) were co-cultured for 24 hours with GC cells treated as above. In OASL-knockdown AGS and MKN45 cells, DCs displayed significantly elevated CD86/CD80 surface expression compared with OXA+si-NC ($P < 0.001$; **(Figure 5g)**). In contrast, DCs co-cultured with OASL-overexpressing HGC27 cells showed reduced CD86/CD80 expression relative to the OXA+Vector group ($P < 0.001$; **(Figure 5g)**).

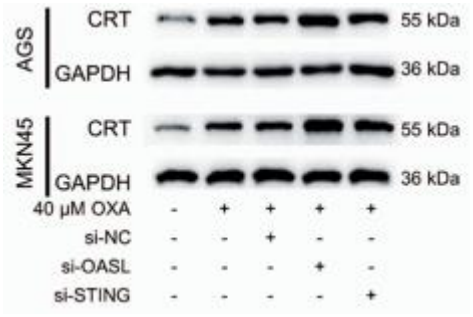

a)

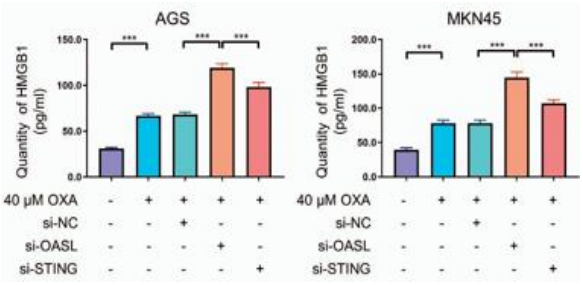

b)

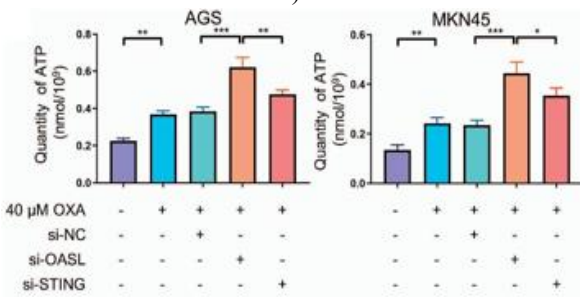

c)

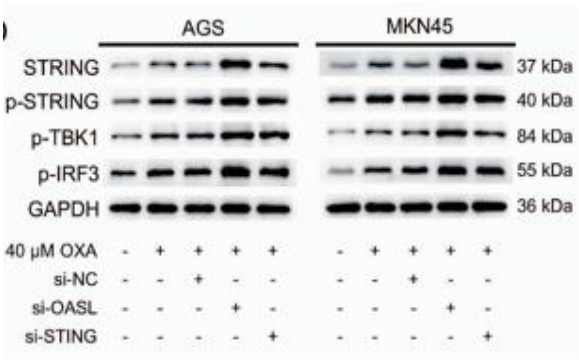

d)

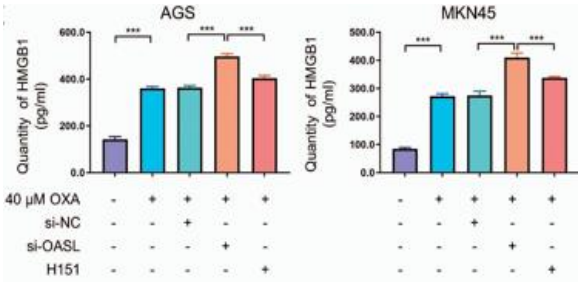

e)

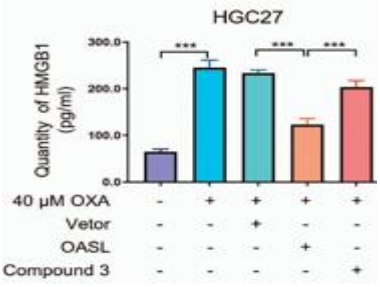

f)

Figure 6. OASL-dependent cGAS-STING signaling pathway to regulate OXA-induced immunogenic cell death

(a) AGS and MKN 45 cells were treated with 40 μM OXA in combination with si-OASL and si- STING for 48 hours,the expression levels of CRT protein in AGS and MKN45 cells were determined by Western blot. (b) AGS and MKN45 cells were treated with 40 μM OXA in combination with si- OASL and si-STING for 48 hours,the statistical plots of HMGB1 content in cell supernatants were detected using ELISA assay.(c) AGS and MKN45 cells were treated with 40 μM OXA in combination with si-OASL and si-STING for 48 hours,the statistical plots of ATP content in cell supernatant detected using ATP kit.(d) AGS and MKN 45 cells were treated with 40 μM OXA in combination with si-OASL and si-STING for 48 hours, and the expression levels of key proteins of the cGAS-STING signaling pathway were

determined by Western blot. (e) AGS and MKN 45 cells were treated with 40 μM OXA in combination with si-OASL and supplemented with H151(an inhibitor of the cGAS-STING signaling pathway) for 48 hours, the statistical plots of HMGB1 content in cell supernatants of cell culture medium were detected using ELISA assay. (f) HGC27 cells were treated with 40 μM OXA combined with overexpressed OASL and supplemented with Compound 3 (an activator of the cGAS-STING signaling pathway) for 48 hours, statistical plot of ATP content in cell supernatant of cell culture medium was detected using ATP kit. The values indicate the mean±standard deviation (SD) of three independent experiments.Statistical significance is indicated as follows: "*" indicates $P < 0.05$, "**" indicates $P < 0.01$, and "***" indicates $P < 0.001$.

Collectively, these findings indicate that OASL negatively regulates the cGAS-STING pathway, thereby modulating ICD and downstream anti-tumor immune activation in response to OXA in gastric cancer cells.

OASL requires the cGAS-STING pathway to modulate oxaliplatin-induced ICD

To determine whether OASL suppresses OXA-induced ICD through the cGAS-STING pathway, rescue experiments were conducted. AGS and MKN45 cells were divided into five groups: control, OXA alone, OXA+si-NC, OXA+si-OASL, and OXA+si-OASL+si-STING, with OXA applied at 40 μM for 48 hours. Compared to the OXA+si-OASL group, co-silencing STING resulted in reduced CRT protein levels ($P < 0.001$; **(Figure 6a)**) and decreased extracellular HMGB1 and ATP ($P < 0.05$; (**Figures 6b and 6c)**). Additionally, the protein levels of STING, P-STING, P-TBK1, and P-IRF3 were significantly diminished in the OXA+si-OASL+si-STING group ($P < 0.05$; **(Figure 6d)**).

Further validation was performed by combining pharmacological modulators of the pathway. AGS and MKN45 cells were treated with OXA (40 μM) under various conditions: control, OXA, OXA+si-NC, OXA+si-OASL, OXA+OASL, and OXA+si-OASL+H151 (STING inhibitor). HMGB1 release and HSP70/HSP90 expression were measured. Addition of H151 reduced HMGB1 in the supernatant and decreased HSP70/HSP90 expression compared to OXA+si-OASL ($P < 0.001$; **(Figure 6e)**). Conversely, in HGC27 cells overexpressing OASL, treatment with the STING agonist Compound 3 increased HMGB1 release and HSP70/HSP90 expression relative to OXA+OASL ($P < 0.001$; **Figure 6f**). These findings indicate that OASL's regulation of OXA-induced ICD is dependent on cGAS-STING signaling.

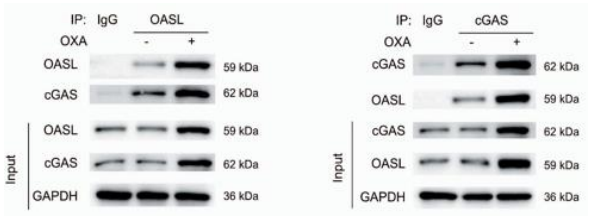

a)

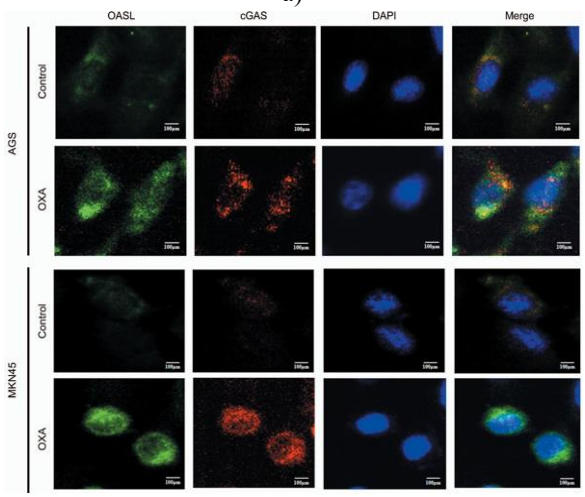

b)

Figure 7. OASL binds to cGAS proteins to inhibit the cGAS-STING signaling pathway
(a) Co-IP results plots for OASL and cGAS(n=3).(b) Immunofluorescence plots verifying the binding of OASL and cGA by adding OXA treatment to AGS and MKN cells(n=3). Scale bar: 100 μm.

OASL interacts directly with cGAS to modulate the cGAS-STING pathway

To further explore the mechanism by which OASL inhibits the cGAS-STING pathway, co-immunoprecipitation (Co-IP) assays were performed, demonstrating a direct interaction between OASL and cGAS proteins **(Figure 7a)**. Immunofluorescence analysis in OXA-treated AGS and MKN45 cells revealed enhanced colocalization and increased expression of OASL and cGAS compared with untreated controls **(Figure 7b)**, suggesting that OASL physically associates with cGAS to modulate downstream signaling.

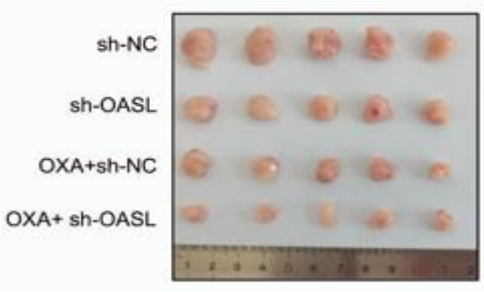
sh-NC
sh-OASL
OXA+sh-NC
OXA+ sh-OASL

a)

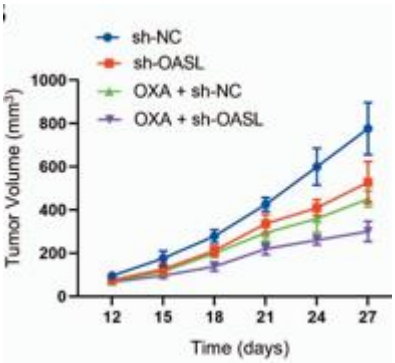
sh-NC
sh-OASL
OXA + sh-NC
OXA + sh-OASL
Tumor Volume (mm³)
1000
800
600
400
200
0
12
15
18
21
24
27
Time (days)

b)

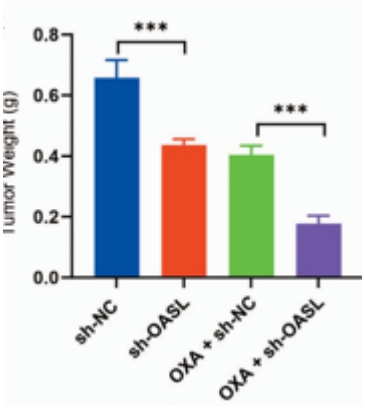
Tumor Weight (g)
0.8
0.6
0.4
0.2
0.0
***
***
sh-NC
sh-OASL
OXA + sh-NC
OXA + sh-OASL

c)

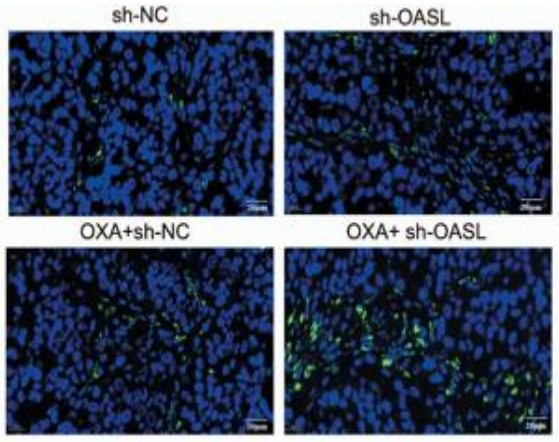
sh-NC
sh-OASL
OXA+sh-NC
OXA+ sh-OASL

d)

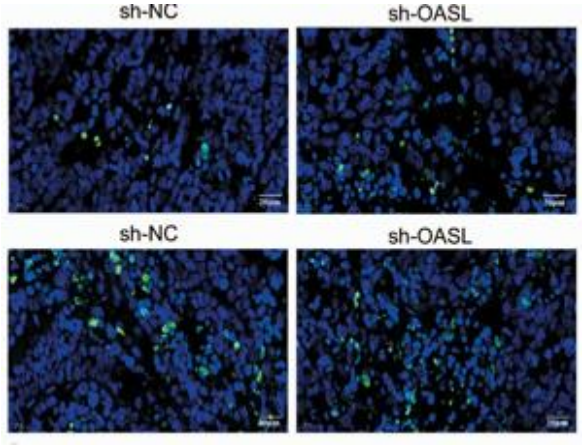
sh-NC
sh-OASL
sh-NC
sh-OASL

e)

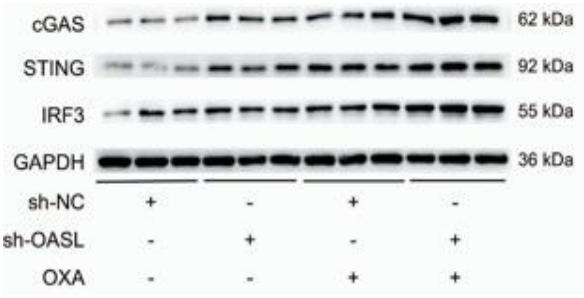
cGAS
62 kDa
STING
92 kDa
IRF3
55 kDa
GAPDH
36 kDa
sh-NC + - + -
sh-OASL - + - +
OXA - - + +

f)

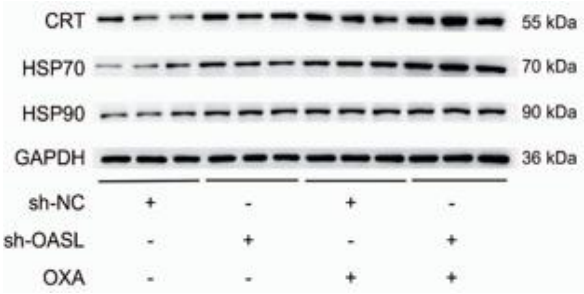
CRT
55 kDa
HSP70
70 kDa
HSP90
90 kDa
GAPDH
36 kDa
sh-NC + - + -
sh-OASL - + - +
OXA - - + +

g)

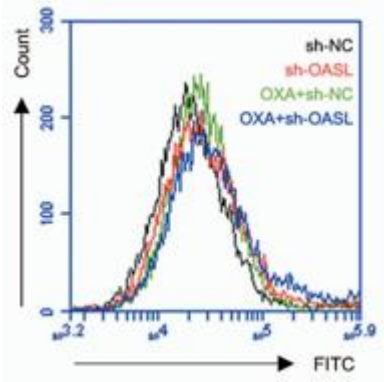
Count
300
200
100
0
sh-NC
sh-OASL
OXA+sh-NC
OXA+sh-OASL
FITC

h)

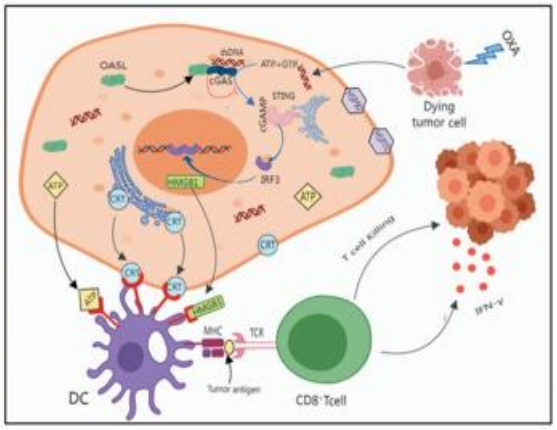

i)

Figure 8. A mouse tumor-bearing model verified that knockdown of OASL improved OXA- induced ICD in GC cells

(a) In vivo tumorigenesis of MFC cells with sh-OASL in mice.(b) Vernier calipers measured the length and width of subcutaneous tumor-bearing tissue of inoculated mice from 12d after inoculation, and plot the growth curve of tumor-bearing tissue.(c) Weight statistical plot of the tumors.(d) Apoptosis and statistics of mouse tumor-bearing tumors detected by TUNEL staining.(e) CD8 expression and statistics of mouse tumor bearing by immunohistochemical fluorescence staining.(f) Expression and statistical plots of key proteins of cGAS-STING signaling pathway determined by Western blot.(g) Expression and statistical plots of the CRT and HSP70 and HSP90 proteins associated with ICD were determined by Western blot.(h)The expression level of CRT on cell membrane was measured using flow cytometry with dead cells. (i) The simulation diagram illustrating the mechanism how OASL exerts its biological effects. The values indicate the mean±standard deviation (SD) of three independent experiments.Scale bar: 20 μm. Statistical significance is indicated as follows: "***" indicates $P < 0.001$.

In vivo verification of OASL's role in oxaliplatin-induced ICD

To validate the in vitro findings, C57/BL6 mice were subcutaneously injected with MFC cells transfected with either sh-OASL or sh-NC and treated with or without OXA. Four experimental groups were established: sh-NC, sh-OASL, OXA+sh-NC, and OXA+sh-OASL. Tumor growth was significantly slower in the sh-OASL group compared with sh-NC, and OXA+sh-OASL exhibited the most pronounced tumor reduction ($P < 0.05$; **(Figures 8a and 8b)**). Tumor weights mirrored this trend, with sh-OASL and OXA+sh-OASL tumors being significantly lighter than their respective controls ($P < 0.01$; **(Figure 8c)**).

Apoptosis assessed by TUNEL staining revealed increased numbers of TUNEL-positive cells in sh-OASL and OXA+sh-OASL tumors compared to controls ($P < 0.01$; **(Figure 8d)**). Immunofluorescence for CD8+ T cells showed enhanced infiltration in sh-OASL and OXA+sh-OASL groups relative to sh-NC and OXA+sh-NC groups ($P < 0.01$; **(Figure 8e)**).

Western blot analysis of tumor tissues confirmed that sh-OASL increased cGAS, STING, and IRF3 protein expression compared to controls, and this effect was further enhanced in combination with OXA ($P < 0.001$; **(Figure 8f)**). Similarly, ICD markers CRT, HSP70, and HSP90 were elevated in sh-OASL and OXA+sh-OASL tumors, and flow cytometry corroborated enhanced CRT surface exposure ($P < 0.05$; **(Figure 8g)**).

Collectively, these in vivo results demonstrate that knockdown of OASL potentiates cGAS-STING pathway activation, enhances OXA-induced ICD, and improves chemosensitivity in gastric cancer.

Gastric cancer (GC) is a prevalent malignant tumor of the digestive system that poses a serious threat to human health. Currently, the primary treatment for GC is surgical resection, often supplemented with radiotherapy and chemotherapy, alongside integrated targeted and immunotherapies. According to the CSCO guidelines, first-line treatment for advanced GC relies on chemotherapy as the central component, which can be combined with immunotherapy or targeted therapy depending on individual clinical circumstances; thus, chemotherapy remains essential for managing advanced GC [7]. Oxaliplatin (OXA) is one of the most frequently administered platinum-based chemotherapeutic agents, acting by forming platinum-DNA adducts that block tumor cell replication and transcription. However, clinical use of OXA has revealed frequent and rapid development of drug resistance [36]. While chemotherapy can effectively reduce tumor burden or temporarily eliminate tumors, prolonged administration often results in multidrug resistance (MDR), a major factor contributing to treatment failure in GC patients [37, 38]. Consequently, strategies to overcome OXA resistance and enhance chemosensitivity remain a critical challenge.

Building on antitumor immunological principles, we hypothesized that OASL plays a key role in regulating OXA chemosensitivity. To elucidate this mechanism, we first assessed whether OXA could induce apoptosis in GC cells in vitro. Our findings demonstrated that OXA inhibited proliferation and promoted apoptosis in GC cells. We then investigated whether immunogenic cell death (ICD) occurred during OXA-induced apoptosis. ICD is largely mediated by damage-associated molecular patterns (DAMPs), such as CRT exposure on the cell surface, HMGB1 release, and ATP secretion, which activate antigen-presenting cells and subsequently trigger effector T cell-mediated antitumor responses [39]. In this study, we observed that the immune response was closely linked to CRT, HMGB1, and ATP, while HSP70 and HSP90 functioned as molecular chaperones [40-42]. Previous studies have shown that bortezomib and anthracyclines can induce surface expression of HSP70 and HSP90, serving as carriers for antigenic peptides [43]. Consistently, our results revealed that OXA increased HSP70 and HSP90 expression in a dose-dependent manner in GC cells, confirming that OXA induces ICD in a dose-dependent fashion.

To further investigate the role of OASL, we modulated its expression in GC cells treated with OXA and measured DAMP release. Knockdown of OASL significantly enhanced OXA-induced ICD, whereas OASL overexpression suppressed it. These results indicate that OASL negatively regulates OXA-induced ICD, underscoring its critical role in maintaining chemosensitivity in GC cells.

To clarify the molecular mechanism by which OASL inhibits OXA-induced ICD, we conducted mRNA sequencing of MKN45 cells in si-NC+OXA and si-OASL+OXA groups. Differential expression and Reactome pathway enrichment analyses revealed significant involvement of second messenger signaling pathways. Notably, in 2011, Russell E. Vance's team identified that STING directly senses c-di-GMP as a DNA sensor in animal cells [44], and subsequent research in 2013 demonstrated that cGAMP can act as a second messenger to activate STING, with cGAS functioning as the upstream synthetic enzyme of cGAMP [45].

The composition and activation of the cGAS-STING signaling axis are now well-characterized: cytosolic double-stranded DNA (dsDNA) binds to cGAS, catalyzing the synthesis of cGAMP from ATP and GTP. Subsequently, cGAMP activates STING, which translocates to the Golgi apparatus and assembles the TBK1-STING-IRF3 complex, ultimately inducing type I interferon production [46, 47]. The cGAS-STING pathway serves as the principal sensor for cytosolic DNA-mediated immune responses [48] and is increasingly recognized for its pivotal role in antitumor immunity. Based on these insights, we hypothesized that OASL exerts its regulatory effects through modulation of the cGAS-STING pathway.

To investigate the functional interplay between OASL and cGAS-STING, we first observed that OXA treatment upregulated cGAS, STING, IRF3, P-STING, P-TBK1, and P-IRF3 in GC cells in a dose-dependent manner. Notably, OASL knockdown potentiated OXA-induced pathway activation, whereas OASL overexpression attenuated it, confirming OASL's inhibitory role. Rescue experiments further substantiated this mechanism: (1) the STING inhibitor H151 reduced HMGB1 release and HSP70/HSP90 expression relative to OXA+si-OASL ($P<0.05$); (2) activation of cGAS-STING via Compound 3 increased these ICD markers compared with OXA+OASL ($P<0.05$); and most importantly, (3) dual knockdown of OASL and STING (OXA+si-OASL+si-STING) reversed ICD indicators, significantly lowering CRT exposure, ATP/HMGB1 release, and phosphorylation of STING/TBK1/IRF3 compared with OXA+si-OASL ($P<0.05$). Collectively, these data demonstrate that OASL modulates oxaliplatin chemosensitivity in GC by controlling ICD through the cGAS-STING signaling pathway.

To further elucidate the regulatory mechanism of OASL on cGAS, we confirmed a direct interaction between OASL and cGAS proteins via co-immunoprecipitation and immunofluorescence, consistent with previous reports showing that OASL binds the DNA sensor cGAS during DNA viral infection, thereby inhibiting interferon induction and enhancing viral replication [49].

Increasing evidence indicates that tumor-infiltrating lymphocytes (TILs) are closely associated with overall survival in GC, with high TIL levels significantly reducing recurrence and mortality [50-52]. CD8+ TILs, as the main component of TILs, are key mediators of antitumor immunity [53] and serve as potential prognostic biomarkers in immune checkpoint therapies for GC. In vivo, OASL knockdown synergized with OXA treatment to activate the cGAS-STING pathway, enhance ICD, and markedly increase CD8+ T-cell infiltration within TILs, directly linking enhanced ICD to augmented TIL infiltration. Importantly, OXA

effectively induced ICD in tumor-bearing mice, and OASL knockdown further amplified this effect.

While established mechanisms of OXA resistance in GC include JUNB-mediated MAPK hyperactivation, EphA2-driven EMT, METTL3-dependent DNA repair and stemness, and LINC00641-regulated autophagy, our study identifies a distinct immunosuppressive axis mediated by OASL. Unlike these intrinsic tumor adaptations, OASL suppresses ICD by directly binding to cGAS and inhibiting the cGAS-STING pathway, thereby blocking dendritic cell maturation and CD8+ T-cell infiltration. This immune-evasion mechanism differs from epigenetic or autophagic resistance pathways, which primarily enhance cell survival. Importantly, OASL knockdown combined with oxaliplatin restored ICD in vivo, highlighting a potential strategy to complement existing approaches targeting conventional resistance mechanisms.

Conclusion

In summary, OASL functions as a critical inhibitor of the cGAS-STING pathway, suppressing OXA-induced ICD in GC cells and thereby reducing chemosensitivity to oxaliplatin.

Acknowledgments: All authors have agreed to the publication of this manuscript.

Conflict of Interest: None

Financial Support: This work was supported by National Natural Science Foundation of China (Grant number 82403927 to Dong Sun), Natural Science Foundation of Shandong Province (Grant number ZR2021MH108 to Jie Chai, ZR2022LZL002 to Sun Dong, and ZR2022MH164 to Longgang Wang), and China Postdoctoral science foundation (Grant number 2022M721445 to Sun Dong), and Hospital-level project of Binzhou People's Hospital (Grant number XJ202202505 to Weizhu Zhao).

Ethics Statement: The study protocol was approved by the ethics committee of Shandong Cancer Institute for Human Study and was conducted according to the principles of the Declaration of Helsinki (Grant number EC-XJS2020-002-01).

References

1. Sung H, Ferlay J, Siegel RL, Laversanne M, Soerjomataram I, Jemal A,et al. Global Cancer Statistics 2020: GLOBOCAN Estimates of Incidenceand Mortality Worldwide for 36 Cancers in 185 Countries.CA: A Cancer Journal for Clinicians. 2021;71(3):209-249.
2. Qi J, Li M, Wang L, Hu Y, Liu W, Long Z,et al.National and subnational trends in cancer burden in China, 2005–20: an analysis of national mortality surveillance data.The Lancet Public Health .2023;8(12):e943-e955.
3. Yoon J, Kim TY, Oh DY. Recent Progress in Immunotherapy for Gastric Cancer.J Gastric Cancer.2023;23(1):207-223.
4. Entezam M, Sanaei MJ, Mirzaei Y, Mer AH, Abdollahpour-Alitappeh M, Azadegan-Dehkordi F, et al.Current progress and challenges of immunotherapy in gastric cancer: A focus on CAR-T cells therapeutic approach.Life Sci.2023; 318:121459.
5. Valkema MJ, Mostert B, Lagarde SM, Wijnhoven BPL, van Lanschot JJB. The effectivity of targeted therapy and immunotherapy in patients with advanced metastatic and non-metastatic cancer of the esophagus and esophago-gastric junction.Updates Surg.2023;75(2):313-323.
6. Zeng H, Chen W, Zheng R, Zhang S, Ji JS, Zou X, et al.Changing cancer survival in China during 2003-15: a pooled analysis of 17 population-based cancer registries.Lancet Glob Health.2018;6(5):e555-e567.
7. Ychou M, Boige V, Pignon JP, Conroy T, Bouché O, Lebreton G, et al. Periopera- tive chemotherapy compared with surgery alone for resectable gastroesophageal adenocarcinoma: an FNCLCC and FFCD multicenter phase III trial.Journal of Clinical Oncology Official Journal of the American Society of Clinical Oncology. 2011;29(13):1715-1721.
8. Nakajima T, Fujii M. What make differences in the outcome of adjuvant treatments for resected gastric cancer? World J Gastroenterol. 2014;20(33): 11567-73.
9. Martinez-Balibrea E, Martínez-Cardús A, Ginés A, Ruiz de Porras V, Moutinho C,Layos L, et al.Tumor-Related Molecular Mechanisms of Oxaliplatin Resistance.Molecular Cancer Therapeutics.2015;14(8):1767-1776.

10. Li S, Wei Y, Sun X, Liu M, Zhu M, Yuan Y, et al. JUNB mediates oxaliplatin resistance via the MAPK signaling pathway in gastric cancer by chromatin accessibility and transcriptomic analysis. Acta Biochim Biophys Sin (Shanghai). 2023;55(11):1784-1796.
11. Wen Q, Chen Z, Chen Z, Chen J, Wang R, Huang C, et al. EphA2 affects the sensitivity of oxaliplatin by inducing EMT in oxaliplatin-resistant gastric cancer cells. Oncotarget.2017;8(29):47998-48011.
12. Wang Y, Hong Z, Song J, Zhong P, Lin L. METTL3 promotes drug resistance to oxaliplatin in gastric cancer cells through DNA repair pathway. Front Pharmacol. 2023;14:1257410.
13. Li H, Wang C, Lan L, Yan L, Li W, Evans I, et al. METTL3 promotes oxaliplatin resistance of gastric cancer CD133+ stem cells by promoting PARP1 mRNA stability. Cell Mol Life Sci. 2022;79(3):135.
14. Hu Y, Su Y, Lei X, Zhao H, Wang L, Xu T, et al. LINC00641/miR-582-5p mediate oxaliplatin resistance by activating autophagy in gastric adenocarcinoma. Sci Rep. 2020;10(1):14981.
15. Jiang J, Zheng X, Xu X, Zhou Q, Yan H, Zhang X, et al.Prognostic Significance of miR-181b and miR-21 in Gastric Cancer Patients Treated with S-1/Oxaliplatin or Doxifluridine/Oxaliplatin.PLoS ONE.2011;6(8):e23271.
16. Zhang LH, Wang Y, Fan QQ, Liu YK, Li LH, Qi XW, et al.Up-regulatedWnt1-inducible signaling pathway protein 1 correlates with poor prognosis and drug resistance by reducing DNArepair in gastric cancer.World Journal of Gastroenterology.2019;25(38):5814-5825.
17. Zhu J, Ghosh A, Sarkar SN.OASL-a new player in controlling antiviral innate immunity.Curr Opin Virol.2015;12:15-19.
18. Donovan J, Whitney G, Rath S, Korennykh A. Structural mechanism of sensing long dsRNA via a noncatalytic domain in human oligoadenylate synthetase 3. Proc Natl Acad Sci USA.2015;112(13):3949-3954.
19. Päri M, Kuusksalu A, Lopp A, Kjaer KH, Justesen J, Kelve M. Enzymatically active 2',5'-oligoadenylate synthetases are widely distributed among Metazoa, including protostome lineage.Biochimie.2014;97:200-209.
20. Zheng S, Zhu D, Lian X, Liu W, Cao R, Chen P. Porcine 2', 5'-oligoadenylate synthetases inhibit Japanese encephalitis virus replication in vitro.J Med Virol.2016;88(5):760-768.
21. Ibsen MS, Gad HH, Andersen LL, Hornung V, Julkunen I, Sarkar SN, et al.Structural and functional analysis reveals that human OASL binds dsRNA to enhance RIG-I signaling.Nucleic Acids Res.2015;43(10):5236-5248.
22. Zhao C, Zheng S, Zhu D, Lian X, Liu W, Hu F, et al.Identification of a novel porcine OASL variant exhibiting antiviral activity.Virus Res.2018;244:199-207.
23. Gao F, Tan Y, Luo H.MALAT1 is involved in type I IFNs-mediated systemic lupus erythematosus by up-regulating OAS2, OAS3, and OASL.Braz J Med Biol Res. 2020;53(5):e9292.
24. Zhang Y, Yu C.Prognostic characterization of OAS1/OAS2/OAS3/OASL in breast cancer.BMC Cancer.2020;20(1):575.
25. Chen S, Sun Z, Zhao W, Meng M, Guo W, Wu D,et al.Oligoadenylate synthetases-like is a prognostic biomarker and therapeutic target in pancreatic ductal adenocarcinoma.Annals of Translational Medicine.2022;10(3):138-138.
26. Zhang L, Jiang Y, Lu X, Zhao H, Chen C, Wang Y,et al.Genomic characterization of cervical cancer based on human papillomavirus status.Gynecologic Oncology.2019;152(3):629-637.
27. Zhao W, Yang H, Liu L, Qu X, Ding J, Yu H,et al.OASL knockdown inhibits the progression of stomach adenocarcinoma by regulating the mTORC1 signaling pathway.The FASEB Journal,2023,37(3):e22824-e22824.
28. Lv J, Wang L, Shen H, Wang X.Regulatory roles of OASL in lung cancer cell sensitivity to Actinidia chinensis Planch root extract (acRoots).Cell Biol Toxicol. 2018;34(3):207-218.
29. Yu C, Xue P, Zhang L, Pan R, Cai Z, He Z,et al.Prediction of key genes and pathways involved in trastuzumab-resistant gastric cancer.World J Surg Oncol. 2018;16(1):174.
30. Greten TF, Wang XW, Korangy F.Current concepts of immune based treatments for patients with HCC: from basic science to novel treatment approaches.Gut. 2015;64(5):842-848.
31. Hato SV, Khong A, de Vries IJ, Lesterhuis WJ. Molecular pathways: the immunogenic effects of platinum-based chemotherapeutics.Clin Cancer Res.2014;20(11):2831-2837.

32. Gatti L, Cassinelli G, Zaffaroni N, Lanzi C, Perego P. New mechanisms for old drugs: Insights into DNA-unrelated effects of platinum compounds and drug resistance determinants.Drug Resist Updat.2015;20:1-11.
33. Bezu L, Gomes-de-Silva LC, Dewitte H, Breckpot K, Fucikova J, Spisek R,et al.Combinatorial strategies for the induction of immunogenic cell death.Front Immunol.2015;6:187.
34. Kepp O, Senovilla L, Vitale I, Vacchelli E, Adjemian S, Agostinis P, et al. Consensus guidelines for the detection of immunogenic cell death. Oncoimmunology.2014;3(9):e955691.
35. Lesterhuis WJ, Punt CJ, Hato SV, Eleveld-Trancikova D, Jansen BJ, Nierkens S,et al.Platinum-based drugs disrupt STAT6-mediatedsuppression of immune responses against cancer in humans and mice.J Clin Invest.2011;121(8):3100-3108.
36. Wei L, Sun J, Zhang N, Zheng Y, Wang X, Lv L, et al.Noncoding RNAs in gastric cancer: implicationsfor drug resistance.Mol Cancer.2020;19(1):62.
37. Saeed A, Park R, Sun W.The integration of immune checkpoint inhibitors with VEGF targeted agents in advanced gastric and gastroesophageal adenocarcino- ma: areview on the rationale and results of early phase trials.Journal of HematologyOncology.2021;14(1):1-11.
38. Song Z, Wu Y, Yang J, Yang D, Fang X. Progress in the treatment of advanced gastric cancer.Tumor Biology.2017;39(7):1010428317714626.
39. Showalter A, Limaye A, Oyer JL, Igarashi R, Kittipatarin C, Copik AJ, et al.Cytokines in immunogenic cell death:Applications for cancer immunotherapy. Cytokine.2017;97:123-132.
40. Kohles N, Nagel D, Jüngst D, Stieber P, Holdenrieder S. Predictive value of immunogenic cell death biomarkers HMGB1, sRAGE, and DNase in liver cancer patients receiving transarterial chemoembolization therapy.Tumour Biol.2012; 33(6):2401-2409.
41. Martins I, Wang Y, Michaud M, Ma Y, Sukkurwala AQ, Shen S,et al.Molecular mechanisms of ATP secretion during immunogenic cell death.Cell Death Differ. 2014;21(1):79-91.
42. Krysko DV, Garg AD, Kaczmarek A, Krysko O, Agostinis P, Vandenabeele P. Immunogenic cell death and DAMPs in cancer therapy.Nat Rev Cancer.2012; 12(12):860-875.
43. Fucikova J, Kralikova P, Fialova A, Brtnicky T, Rob L, Bartunkova J, et al.Human tumor cells killed by anthracyclines induce a tumor-specific immune response. Cancer Res.2011;71(14):4821-4833.
44. Burdette DL, Monroe KM, Sotelo-Troha K, Iwig JS, Eckert B, Hyodo M, et al. STING is a direct innate immune sensor of cyclic di-GMP.Nature.2011; 478(7370):515-518.
45. Wu J, Sun L, Chen X, Du F, Shi H, Chen C,et al.Cyclic GMP-AMP is an endogenous second messenger in innate immune signaling by cytosolic DNA.Science.2013;339,(6121):826-830.
46. Chen Q, Sun L, Chen ZJ.Regulation and function of the cGAS-STING pathway of cytosolic DNA sensing.Nat Immunol.2016;17(10):1142-1149.
47. Galluzzi L, Vanpouille-Box C, Bakhoum SF, Demaria S.SnapShot: cGAS-STING Signaling.Cell.2018;173(1):276-276.
48. Fang R, Jiang Q, Yu X, Zhao Z, Jiang Z. Recent advances in the activation and regulation of the cGAS-STING pathway.Adv Immunol.2022;156:55-102.
49. Ghosh A, Shao L, Sampath P, Zhao B, Patel NV, Zhu J, et al.Oligoadenylate- Synthetase-Family Protein OASL Inhibits Activity of the DNA Sensor cGAS during DNA Virus Infection to Limit Interferon Production.Immunity.2019;50(1): 51-63.
50. Hu K, Wang S, Wang Z, Li L, Huang Z, Yu W, et al.Clinicopathological risk factors for gastric cancer: a retrospective cohort study in China.BMJ Open. 2019;9(9):e030639.
51. Shen Q, Polom K, Williams C, de Oliveira FMS, Guergova-Kuras M, Lisacek F,et al.A targeted proteomics approach reveals a serum protein signature as diagnostic biomarker for resectable gastric cancer. EBioMedicine. 2019;44:322-333.
52. Zhou B, Zhou Z, Chen Y, Deng H, Cai Y, Rao X, et al. Plasma proteomics-based identification of novel biomarkers in early gastric cancer.Clinical Biochemistry.2020;76:5-10.
53. Bang CS, Lee JJ, Baik GH.Diagnostic performance of serum pepsinogen assay for the prediction of atrophic gastritis and gastric neoplasms.Medicine.2019; 98(4):e14240.